

Z2P: Instant Rendering of Point Clouds

GAL METZER, Tel Aviv University
 RANA HANOCKA, Tel Aviv University
 RAJA GIRYES, Tel Aviv University
 NILOY J. MITRA, University College London, Adobe Research
 DANIEL COHEN-OR, Tel Aviv University

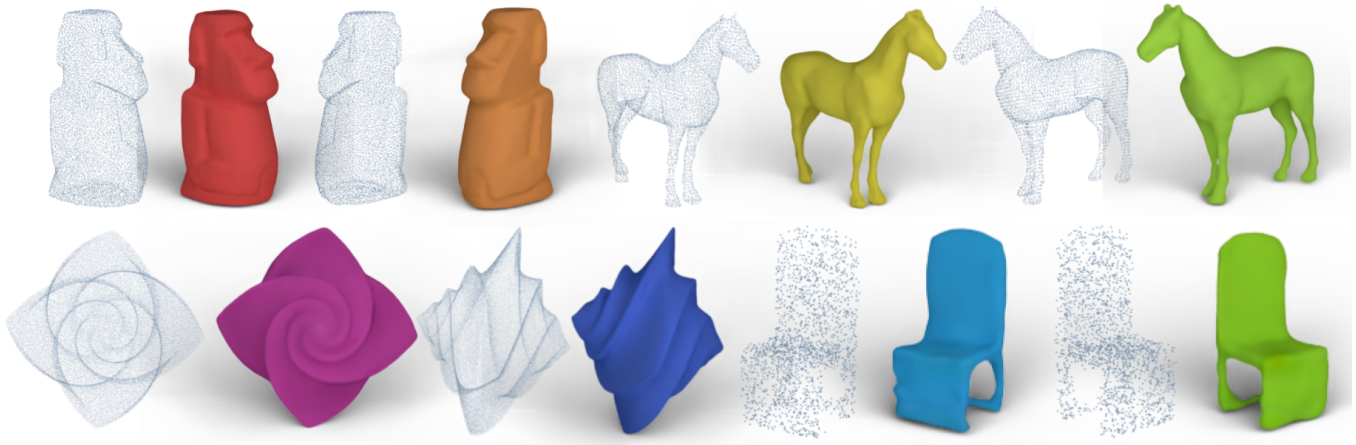


Fig. 1. Point cloud inputs and resulting renderings using our Z2P, conditioned on different colors and lighting positions.

We present a technique for rendering point clouds using a neural network. Existing point rendering techniques either use splatting, or first reconstruct a surface mesh that can then be rendered. Both of these techniques require solving for global point normal orientation, which is a challenging problem on its own. Furthermore, splatting techniques result in holes and overlaps, whereas mesh reconstruction is particularly challenging, especially in the cases of thin surfaces and sheets.

We cast the rendering problem as a conditional image-to-image translation problem. In our formulation, *Z2P*, *i.e.*, depth-augmented point features as viewed from target camera view, are directly translated by a neural network to rendered images, conditioned on control variables (e.g., color, light). We avoid inevitable issues with splatting (*i.e.*, holes and overlaps), and bypass solving the notoriously challenging surface reconstruction problem or estimating oriented normals. Yet, our approach results in a rendered image *as if* a surface mesh was reconstructed. We demonstrate that our framework produces a plausible image, and can effectively handle noise, non-uniform sampling, thin surfaces / sheets, and is fast.

Authors' addresses: Gal Metzger, Tel Aviv University; Rana Hanoeka, Tel Aviv University; Raja Giryes, Tel Aviv University; Niloy J. Mitra, University College London, Adobe Research; Daniel Cohen-Or, Tel Aviv University.

Permission to make digital or hard copies of all or part of this work for personal or classroom use is granted without fee provided that copies are not made or distributed for profit or commercial advantage and that copies bear this notice and the full citation on the first page. Copyrights for components of this work owned by others than ACM must be honored. Abstracting with credit is permitted. To copy otherwise, or republish, to post on servers or to redistribute to lists, requires prior specific permission and/or a fee. Request permissions from permissions@acm.org.

© 2021 Association for Computing Machinery.
 0730-0301/2021/6-ART \$15.00
<https://doi.org/10.1145/nnnnnnn.nnnnnnn>

1 INTRODUCTION

Point clouds are a popular and flexible representation of 3D shapes. A slew of works have successfully employed deep neural networks to synthesize point clouds, for shape synthesis [Achlioptas et al. 2018; Li et al. 2018; Yang et al. 2019; Hertz et al. 2020; Gal et al. 2020], upsampling [Yu et al. 2018b; Yifan et al. 2019b], consolidation [Yu et al. 2018a; Metzger et al. 2020], shape completion [Yuan et al. 2018], denoising [Rakotosaona et al. 2020], among others. Thus generating an increasing demand for a fast and effective point cloud rendering technique. Yet, neurally synthesized point clouds do not contain a globally consistent normal orientation (since standard loss functions do not trivially enable normal regression [Metzger et al. 2021]), which is a prerequisite for rendering them.

Since points are zero-dimensional entities, they cannot be rendered directly. One approach enables point rendering by converting each point into a local tangent patch (*i.e.*, splats) [Zwicker et al. 2001; Botsch and Kobbelt 2003]. Since point samples are irregular and unstructured, different heuristics for deciding the size of local spats will inevitably lead to holes and overlaps. Moreover, these techniques must also take into account hidden surface removal. In addition, global point normal *orientation* is a necessary requirement for point splatting, which is a challenging problem in and of itself [Mitra and Nguyen 2003; Huang et al. 2009].

A more meticulous approach is to first reconstruct a mesh surface from the input point samples [Kazhdan et al. 2006; Kazhdan and Hoppe 2013] and then render the mesh. However, reconstructing a surface is a notoriously difficult problem. Such an approach appears

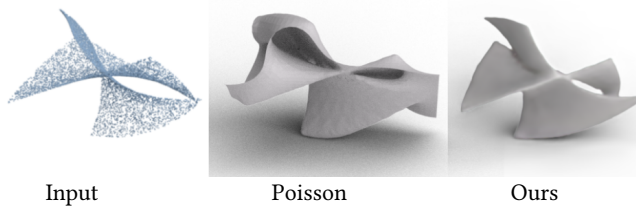


Fig. 2. Sheets are especially hard to orient, reconstruct, and may be unprintable. Popular techniques such as Poisson reconstruction [Kazhdan et al. 2006] are not well defined in these cases (due to the open surface and poor normals). Our method, which operates on raw point clouds, can handle such cases as it does not rely on oriented normals or other surface attributes.

to be *overkill* if the end goal is to simply render the point set. Further, it inherits the problems of any reconstruction algorithm. For example, neural synthesized point clouds lack normal orientation and often contain interior points, resulting in poor reconstruction results. Moreover, surface reconstruction is unstable and not well defined in the case of thin surfaces and sheets.

In this work, we present *Z2P*, a technique for directly rendering sparse noisy point clouds (*as if* the mesh was reconstructed) using a neural network. Our network learns a mapping from point clouds to a rendered image of the underlying mesh surface. We argue that if the final goal is to generate an image (*i.e.* render), then we can bypass the need to orient point normals or reconstruct a surface mesh, and obtain a plausible rendering in less time. Our technique is based on a surprisingly simple network architecture, which enables easy control of view direction, colors, and ambient shadows. Specifically, we achieve a complete disentanglement of the shape geometry from the rendering parameters (*e.g.*, color, shadow).

We cast the rendering problem as an image-to-image translation problem whereby z-buffers, *i.e.*, depth-augmented point features as viewed from target camera view, are directly translated by a neural network to rendered images, conditioned on control variables (*e.g.*, color, light). We inject rendering controls, such as light position and colors as an input condition to the network using adaptive instance normalization. The convolutional nature of the network enables learning a mapping at the patch level, which would ignore long-distance relationships that are crucial for shadows. However, by leveraging a positional encoding, we break the locality and gain non-local shading effects.

Our network is trained on automatically generated pairs of point clouds and rendered meshes, and only requires training on a few unique meshes to achieve generalization.

We generate a copious amount of paired data from each mesh, by applying random lighting, color, and rotation augmentations. During inference our method can render plausible images from point clouds where the ground-truth is unknown (*i.e.*, noisy point clouds from neural networks or scanning devices), bypassing the challenging reconstruction or point normal orientation problem altogether. Moreover, it is significantly faster than the rendering engine it was trained on: our rendering phase takes under 1 second, while the engine takes over 10 seconds.

We show that our method can act as an effective, quick-and-dirty point cloud rendering technique, while still providing useful control.

We demonstrate our approach can successfully handle noise, non-uniform sampling, and in particular thin surfaces and sheets (see Figure 2). Our experimental evaluations show that our technique is comparable or better than existing techniques, and is considerably faster.

2 RELATED WORK

Surface Reconstruction. Reconstructing a surface mesh from point clouds is a long standing problem in computer graphics that has been studied extensively for over 20 years [Berger et al. 2017]. A common approach triangulates a set of points [Edelsbrunner and Mücke 1994; Bernardini et al. 1999]. Alternatively, an implicit function can be built from the point cloud and normals, and the surface mesh is extracted by finding the zero-crossings [Hoppe et al. 1992; Kazhdan et al. 2006; Kazhdan and Hoppe 2013]. Surface reconstruction can also be obtained using a mesh deformation technique, where an initial mesh is incrementally displaced to fit an input point cloud [Sharf et al. 2006; Hanocka et al. 2020].

A common prerequisite for surface reconstruction is calculating a globally consistent normal orientation [Mitra and Nguyen 2003; Guerrero et al. 2018; Schertler et al. 2017]. Though some techniques, such as [Mullen et al. 2010; Hanocka et al. 2020] can reconstruct surfaces with unoriented normals. Triangulation techniques (such as ball-pivot [Bernardini et al. 1999]), handle thin sheets well, yet inevitably lead to undesirable holes in the reconstruction. On the other hand, implicit surface reconstruction (such as Poisson [Kazhdan et al. 2006; Kazhdan and Hoppe 2013]) tend to handle holes better, yet occupancy is not-well defined in the case of sheets. Finally, this route is computationally expensive since it requires both reconstructing a surface and then rendering an image.

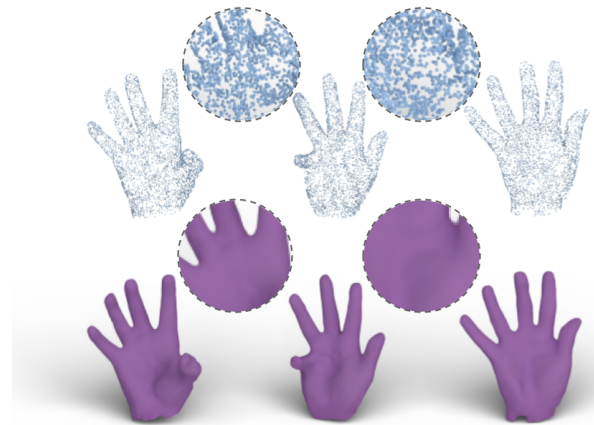


Fig. 3. Our method can directly render point clouds with non-uniform sampling. Note the self shadow effects on the palm of the left example.

Deep Rendering. Since the introduction of the rendering equation [Kajiya 1986], many works have proposed techniques to speedup the rendering process, for example, using *deferred shading* [Saito and Takahashi 1990] to produce a render from 2D G-buffers (*e.g.*, depth image, normal maps, etc). Recently, deep learning has been

used to perform deferred shading [Nalbach et al. 2017] which calculates the G-buffer from the complete 3D scene. However, estimating these maps (e.g., occlusions, light and normal information) is non-trivial for point clouds. RenderNet [Nguyen-Phuoc et al. 2018] learns to produce 2D images from a 3D voxel representation of the shape. Adopting this approach to point clouds is wasteful as it requires creating a voxelized volume (reducing the resolution down to $64 \times 64 \times 64$), as well as require oriented normals. Hermosilla et al. [2019] learns to shade surfaces using deep neural networks and G-buffers, which is a faster alternative than path-tracing. Note that we do not have access to G-buffer information in our case.

Neural point cloud rendering has been studied in [Kolos et al. 2020; Dai et al. 2020; Aliev et al. 2019]. These works mainly focus on dense point clouds of scenes captured from real RGBD scanners, and contain per-color attributes. This leads to systems where the lighting, normal, material properties have been aggregated into a single RGB value per-point. Instead, in this work, we focus on the problem of rendering neurally synthesized point clouds, which do not contain globally consistent oriented normals. Moreover, our system achieves complete disentanglement of lighting, color, and ambient shadows. Recently, [Chen et al. 2021] proposed a controllable neural rendering pipeline for neural 3D shapes represented by neural implicit.

An orthogonal line of works propose differential rendering [Yifan et al. 2019a; Chen et al. 2019] techniques for a plug-and-play module in deep learning architectures. Different than the objective of this work, these works are used to perform shape reconstruction or inverse rendering (i.e., recovery of unknown 3D scene and lighting).

3 METHOD

We formulate the rendering task as an image-to-image translation from z-buffers of projected point clouds to rendered images, conditioned on the rendering settings. Our framework is simple, yet effective. We automatically generate simulated training data to train a fully-convolutional network to learn a mapping from point cloud z-buffers to rendered mesh images. We inject rendering control through Adaptive Instance Normalization (AdaIN) [Huang and Belongie 2017] layers, enabling a disentangled representation of rendering parameters and shape.

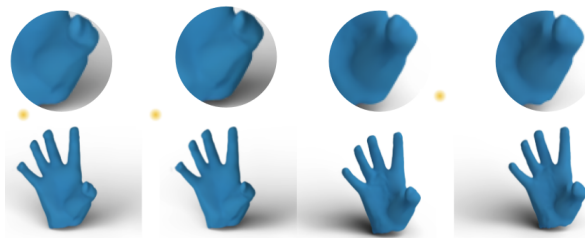


Fig. 4. Self shadow effects are plausibly generated with our method. Light position is visualized in yellow.

Synthesizing shadows requires long range interactions between pixels (see Figures 4 and 8). This is achieved by the U-Net [Ronneberger et al. 2015] structure which takes into account various scales of the input. Yet, in order to enable the network to effectively

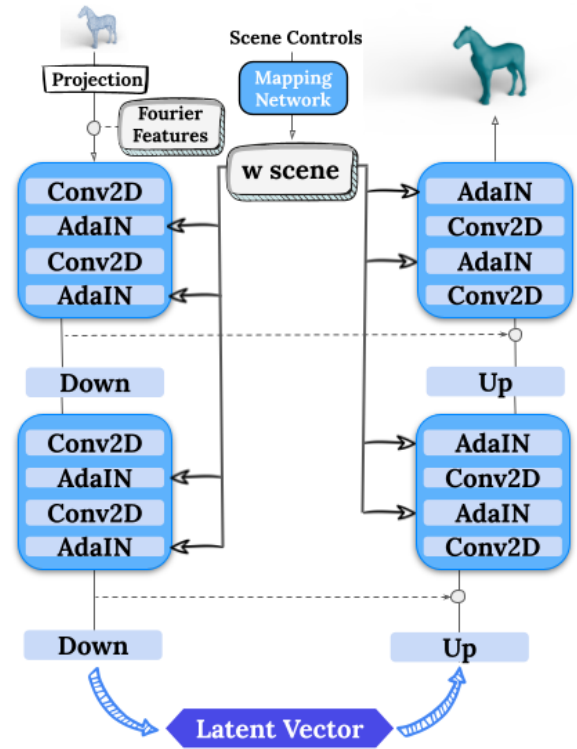


Fig. 5. Overview. We project the point cloud into a 2D z buffer image, which is the input to our network. We append positional encoding (Fourier features) in order to model long-range effects required to generate shadows. We inject scene controls into AdaIN after each convolutional layer, enabling control of the light and color in the scene.

process the light direction, we break the translational symmetry of the convolutions by appending positional encoding to the input. During inference, we use real point clouds (i.e., noisy point clouds obtained from neural networks or scanning devices) to obtain a plausible quality image, rendered in under a second, bypassing the challenging surface reconstruction or point normal orientation problem altogether.

3.1 Point cloud projection

We use a 2D z-buffer projection of the point cloud as input to our network. Xie et al. [2021] demonstrated a similar projection was useful for their adversarial loss. Each point in the point cloud p is projected onto the nearest 2D image coordinate (u_p, v_p) , with an intensity value proportional to the depth d_p , i.e., distance to the image plane. The projection is a perspective transformation according to the camera pinhole model with extrinsic (camera location) and intrinsic (e.g., focal length) parameters. Pixels in the 2D image plane that do not correspond to any 3D points receive an intensity of 0, while other pixels receive an intensity value according to

$$z(u_p, v_p) = e^{-\frac{d_p - \alpha}{\beta}}, \quad (1)$$

where α and β are hyperparameters that we fix once throughout training, inference and all experiments. The width of the intensity

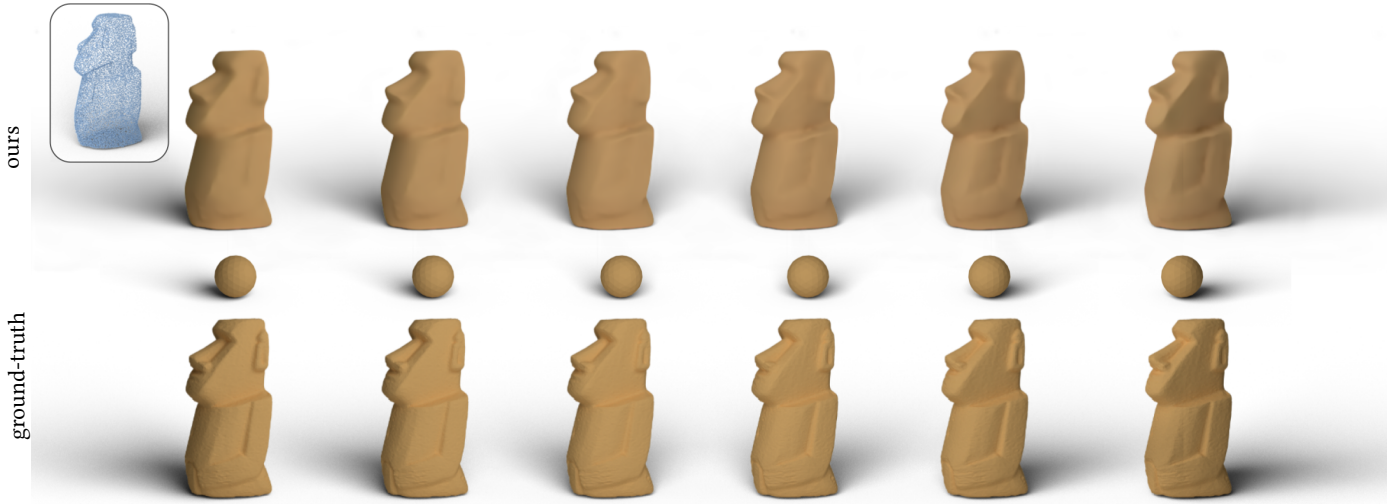


Fig. 6. Lighting control. Top: our rendered result conditioned on slowly changing light position produces a smooth transformation of the shade and objects lighting. Bottom: Ground truth mesh renderings under corresponding conditions. The shaded sphere helps visualizing the light direction.

values for each points' 2D projection on the image is within a 5×5 window. In the case where multiple points are assigned to the same pixel, we use only the closest one to determine the intensity.

The intuition behind our z-buffer image is that points far away receive a value approaching the background intensity, whereas close points are exponentially brighter than occluded ones. This makes 2D features consistent with the rendering requirements, since far points are usually occluded, which should result in an intensity value that is close to background and much lower than points which are in front of it. Note that our z-buffer image may contain backfacing points, since we do not use oriented point normals. Despite this, we observe that our network is able to cope with such hidden surfaces well.

3.2 Training Data Generation

Our training data is automatically generated using Blender 3D engine [2021], which provides explicit control over the rendering parameters. We sample meshes to produce corresponding pairs of point cloud and mesh data. In order to generate a large amount of geometric variety using only a small number of unique meshes, we apply random rotations and create different point cloud instances from the same mesh. Note that due to the convolutional nature of the network, which shares weights across patches of the input z-buffer, the *effective number* of training examples is larger than the number of pairs of input images.

For each pair of point cloud and underlying mesh pair, we randomly select a color and light location which is used to automatically render an image using Blender Cycles engine. The light is modeled using a flat emission surface with a floor plane for catching shadows and ambient light.

This results in many pairs of training inputs (z_i, s_i) and outputs r_i , where z_i is the 2D projection of the point cloud, s_i is a vector containing the settings (color and light position), and r_i is the corresponding blender rendered image.

The training data is composed of 20 unique meshes each augmented 400 times with rotation, color, and lighting position. Each mesh has 10 corresponding point clouds that were sampled from it. This results in 80K pairs of training examples.

3.3 Network architecture

We formulate our rendering task as an image-to-image translation from z-buffers to rendered images (with an alpha channel for matting). However, this is not a simple image-to-image setup as the target rendering is conditioned on the given color and light position. To solve the rendering control problem, we propose a modified U-Net [Ronneberger et al. 2015] architecture, where we add AdaIN layers to control the color and light position, and use positional encoding to produce accurate shadows. Below, we describe each of these added components. In Section 4, we show the importance of these components through an ablation study.



Fig. 7. Color control. We keep a constant light and view angle, while continuously varying the input color.

Rendering control Our architecture enables independent control of both the object color as well as light position in its rendering. This disentanglement can be seen in figures 7 and 6. We inject the color to the network as a 3-dimensional vector, which

defines the RGB values of the target shape. The light position is given as a 3-dimensional vector corresponding to the light position in spherical coordinates with respect to the camera. The two vectors are concatenated to produce the settings vector $s \in \mathbb{R}^6$. We map the settings vector $s \in \mathbb{R}^6$ to a higher dimensional vector $w \in \mathbb{R}^{512}$ by an MLP mapping network. The vector w is used to produce the mean and standard deviation that are used by the AdaIN layers. Notice that while w is shared across all AdaIN layers, each of them uses a different (learned) affine transform to control its parameters. This dependence on the light and color through AdaIN allows controlling the scene setting.

Adaptive Instance Normalization (AdaIN) The original U-Net uses batch normalization after each convolution operation. However, to control the color and shadows of the resulting image, we replace batch normalization with AdaIN layers. These layers normalize the feature map from the prior convolution operation. This was also shown to be an effective technique for controlling global style effects in [Karras et al. 2019].

Each AdaIN layer ADA_i has a target feature length of size f_i . In order to use the global vector w , each AdaIN layer contains two additional affine transformations $A_{\beta,i}, A_{\gamma,i}$ that receive an input of size 512 and output a vector of size f_i .

Formally, each AdaIN layer takes as input a feature map x of size $H \times W \times f_i$ and the vector w . The affine transformation is used to calculate $\beta_i = A_{\beta,i} \cdot w$ and $\gamma_i = A_{\gamma,i} \cdot w$, and the feature map x is normalized according to Equation 2 below, where $\mu(x)$ and $\sigma(x)$ are the mean and standard deviation over the spatial dimensions per each channel.

$$\hat{x} = \gamma_i \cdot \left(\frac{x - \mu(x)}{\sigma(x)} \right) + \beta_i \quad (2)$$

Positional encoding U-Net is a fully convolutional network which means it has a limited receptive field, and is translation equivariant. The light position is used to control shadows. This requires long range interactions between pixels, and should not be translation equivariant. For example, when lifting an object in the vertical direction, shadows should remain at the bottom of the image, as the object moves farther away from the bottom floor plane (see Figure 8).



Fig. 8. Shadow effects require positional encoding. During inference, we move the object location upwards (without having trained on this type of data). Observe how the positional encoding correctly learns the shadow interactions, keeping the floor plane in the correct location.

To allow for long interactions and break the translational symmetry, we append positional encoding features to the input image that depend on the pixel location. This enables the convolution filters to grasp the global context. We use random Fourier features, which has been successful at modeling both short and long interactions [Tancik et al. 2020].

Formally, each pixel gets a normalized coordinate value (u_i, v_i) in the range $[0, 1]$. At the beginning of training, ten $\{\omega_j\}$ values are sampled from a uniform distribution $\omega_j \sim U[0, 10]$, to produce 40 features for each pixel of the form:

$$enc_i = [\{\sin(\omega_j \cdot u_i)\}_j, \{\sin(\omega_j \cdot v_i)\}_j, \{\cos(\omega_j \cdot u_i)\}_j, \{\cos(\omega_j \cdot v_i)\}_j] \quad (3)$$

Each encoding enc_i is concatenated to its corresponding pixel in the z-buffer, which creates additional input features.

3.4 Losses

Our network is trained using a combination of simple reconstruction losses. The network produces a 4-dimensional image, three color channels (for RGB) as well as an alpha channel for transparency. We use an $L2$ loss between the network-predicted color image and the ground-truth color image. We also calculate the magnitude of the three color channels (pixel-wise) for both images and calculate the $L1$ -norm between them. We also compute the $L1$ distance between the ground truth and predicted alpha map intensities.

4 EXPERIMENTS

We performed various experiments to validate our network performance as well as compare to existing surface reconstruction techniques. We demonstrate the ability to generalize on point clouds, where the ground-truth surface is unknown, such as real scans, as well as on point clouds that were synthesized from neural networks. We justify various components of our network architecture and perform run-time comparisons. All results in this paper are shown on held out validation or test set examples. There are extended results and evaluations in the supplementary material and video.

4.1 Rendering control

We control the rendered result by modifying different settings: light position, color, and viewing angle. For example, in Figure 7 (more in supplemental) we control the color of the rendered result. In Figure 6 we move the light position in the horizontal direction, which changes the ambient shading on the object as well as the shadows on the ground (yet the color is held constant). We also show the rendered result from multiple view points in Figure 9, while holding light position and color constant. See supplemental video for temporal animations of modifying different rendering controls, as well as the supplemental material.

4.2 Handling noisy inputs

Depending on the use case, one may want to disregard noise, even if it is part of the input. We trained our model with examples containing uniform noise to produce a type of *denoising* renderer. To test the ability to disregard noise, we added an increasing level of Gaussian noise during inference (different than the noise we trained on), in Figure 10. The last row contains the results on Z2P trained with



Fig. 9. Point clouds can be rendered from multiple views while producing a coherent result with respect to both color and shadows.

uniform noise, and the second to last row is Z2P trained on clean data. The noise-removal version renders results that are noticeably smoother than the baseline Z2P, however this may come at the cost of over-smoothing fine details, since they can be attenuated in the presence of noise.

4.3 Robustness to sampling

We show robustness to different types of sampling methods in Figure 11. Note, that despite only being trained on uniformly sampled meshes, our method is able to generalize to different sampling methods, as well as noise from neural synthesized point networks and real scanning devices.

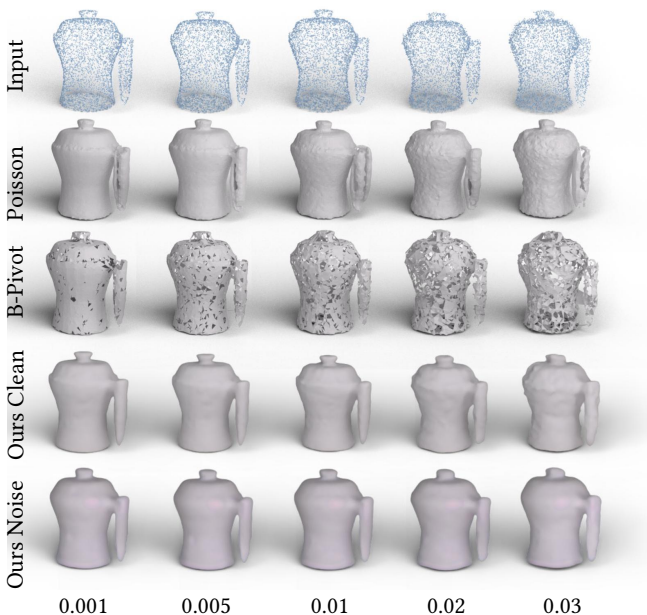


Fig. 10. Handling noisy inputs. We compare against different approaches for rendering a noisy point cloud with increasing levels of Gaussian noise (standard deviation at the bottom). The last row shows results of our network trained with examples corrupted with uniform noise.

We also evaluate the ability of our method to cope with point clouds at different scales, which results in a different point density on the z-buffer image in the supplemental material.

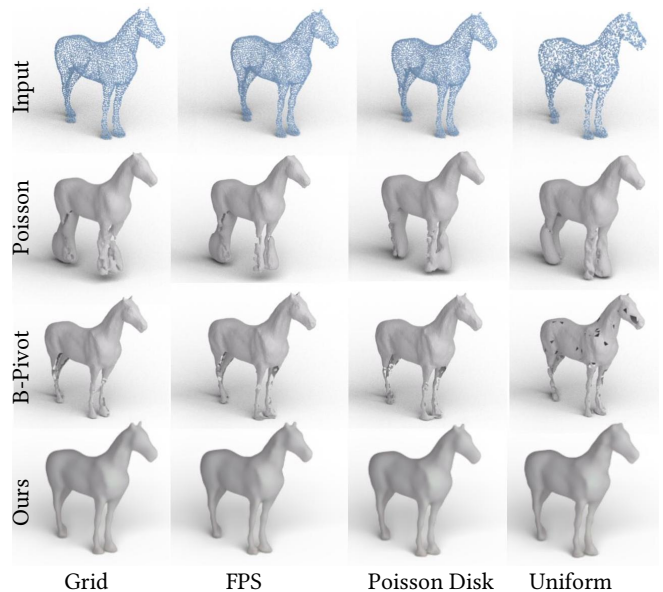


Fig. 11. Robustness to different point sampling methods. Poisson reconstruction and ball-pivot (top, middle rows respectively) vary in quality across different sampling methods, our method is able to produce a high quality consistent rendering of the point cloud.

4.4 Generalization

We demonstrate the ability of our technique to render images from point clouds where the ground-truth underlying surface is unknown. Such an example is point clouds synthesized from neural networks. These are interesting since they are challenging for surface reconstruction methods [Metzger et al. 2021], since they do not contain normal information and often have inner points and single sheets.

In Figure 15 and in the supplementary, we show our ability to robustly handle these challenging cases, without oriented normals

and with the unknown noise distribution. Future deep learning approaches may use our work to better visualize the generated shapes.

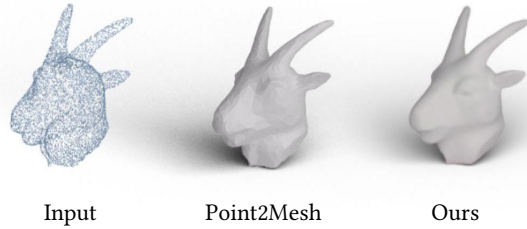


Fig. 12. Comparison to [Hanocka et al. 2020]. Though Point2Mesh also produces good results, it requires a long time to converge (30-60 minutes), compared to our result that is obtained in seconds.

We also compared against Point2Mesh [Hanocka et al. 2020] which also does not require normal orientation, in Figure 12. Additional comparisons can be found in the supplementary.

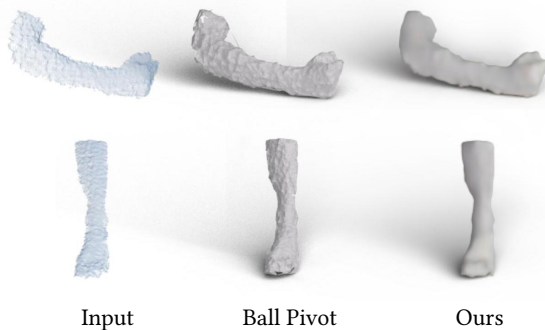


Fig. 13. Results of rendering single view point clouds obtained from Real Sense depth scanner.

Scans acquired from sensor devices, are usually obtained as a single occluded view. These scans are not well defined for Poisson reconstruction, but can be used with an explicit triangulation method like ball pivot (which tends to introduce noise). Figure 13 shows results of a single view scan obtained from a low-end *Intel RealSense SR300* scanner. We also show results on a lidar scanner, which contains an open surface which is especially challenging for surface reconstruction techniques, such as Poisson 14.

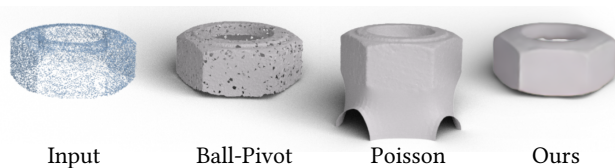


Fig. 14. Results on real lidar scanned data, which contains holes, noise and open surfaces.

4.5 Timing comparison

Table 1 shows the run-time of each individual component in our method. The table shows the timings for: projecting the point cloud onto the 2D coordinate plane (*project*), calculating the z-buffer intensity (*z-buffer*), forward pass through the network (*forward*), and the average overall time it takes for one example (*avg per example*). Rendering a point cloud from start to finish takes under three seconds for a point cloud of size 5k, where the most expensive computation is the z-buffering process. Since the z-buffering code is written in Python, this part can be significantly accelerated using GPU and C++. Training our method takes around 24 hours on a single GTX 1080 Ti GPU. Rendering the train and validation set takes 48 hours (using a single GPU with Blender).

Rendering an image from point clouds by first estimating a reconstruction is computationally expensive. As shown in Table 2, Reconstruction requires estimating the point normals and propagating their orientation (~3 seconds), running the reconstruction algorithm itself (~1 or ~10 seconds), and then rendering the result with blender (~10 seconds). In total, Poisson reconstruction and ball pivot take 13.85 and 23.92 seconds, respectively, whereas our technique on the same point cloud takes less than 3 seconds.

4.6 Architecture ablation

The design choices of our architecture are explained through several experiments. We control the rendering through AdaIN, which has been shown to be a powerful tool for controlling style parameters.

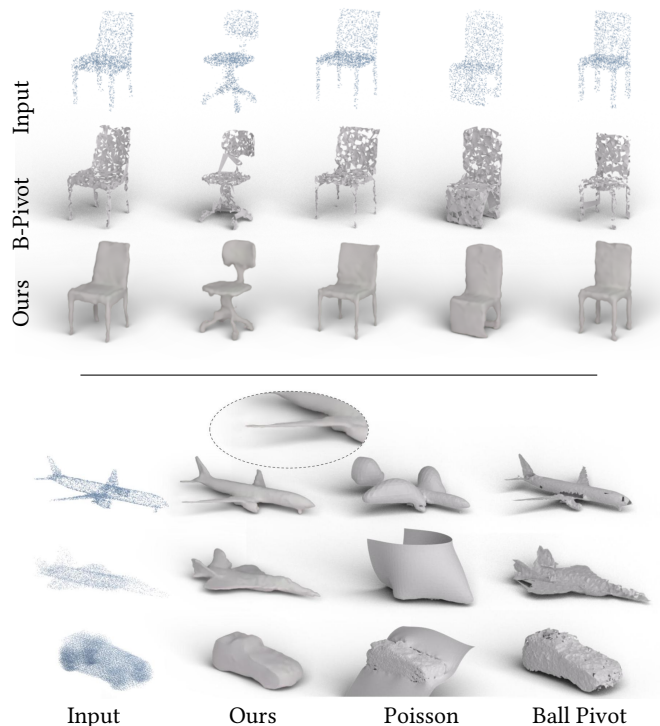


Fig. 15. Our results on different chairs, planes, and cars generated by [Cai et al. 2020]. Poisson reconstruction was not able to produce a meaningful result for the chairs with thin surfaces in the top row.

Table 1. Run time break down. Rendering a point cloud from start to finish using our method takes under 3 seconds. The z-buffer operation takes almost all the time, which is written in unoptimized Python code.

batch size	project ms	z-buffer sec	forward ms	avg per example sec
1	<0	2.60	20	2.62
2	10	5.04	40	2.54
3	10	7.88	60	2.65
4	10	10.70	80	2.69
5	20	13.28	110	2.68
6	20	17.48	120	2.93

Table 2. Run time break down for surface reconstruction approaches. In total, Poisson reconstruction and ball pivot take 13.85 and 23.92 seconds, respectively, whereas our technique on the same point cloud takes less than three seconds (Table 1).

steps [sec]	Poisson	B-pivot
normal estimation	2.76	2.76
reconstruction	10.63	1.03
render	10.53	10.06
total time	23.92	13.85

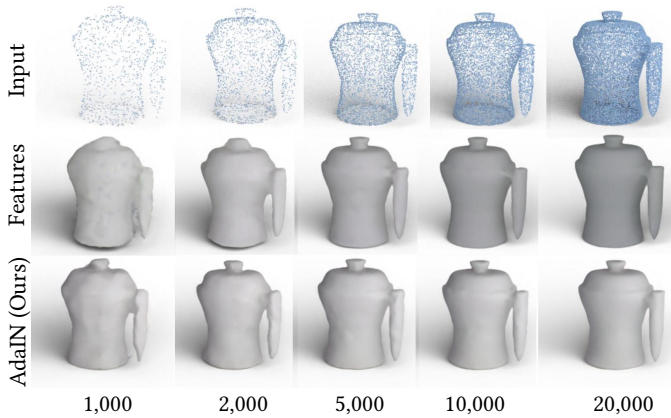


Fig. 16. The rendering control vector as extra input features leads to an inconsistent lighting color result with respect to the input density.

We compare it to a feature-baseline, where instead of injecting the rendering settings through AdaIN, we create a variant of our network which appends the rendering settings as extra input features (repeated for every input z-buffer pixel). Note how in Figure 16, the AdaIN version maintains a consistent color regardless of sampling density. By injecting controls at a global scale with AdaIN, which only changes second order feature map statistics, we obtain a framework with better style consistency and control.

We also test the impact of the positional encoding. Figure 8 shows that it is necessary for correctly modeling the long range interactions needed to generate shadows.

5 CONCLUSIONS AND FUTURE WORK

We have presented a neural rendering technique for point clouds. We refer to this technique as instant rendering as we bypass the cumbersome common step of explicitly converting the point cloud to a continuous surface prior to rendering. Moreover, our instant rendering relaxes the need to compute or use normals; instead, we directly project points to a simple z-buffer. In its basic form, our technique is a *conditional* image-to-image convolutional network. However, a vanilla fully convolutional network would learn translation at the patch level, and ignore long-distance relations. We showed that by injecting positional encoding, we break the locality and gain non-local shading effects.

Limitations and future directions. Our rendering may not always be completely accurate, for example, nearby points in Euclidean space may be rendered as touching, when in fact they are far in geodesic proximity (see Figure 17). Our renderer has less control than a typical rendering engine. This might be addressed by incorporation textures, materials, and other types of lighting models in the learning procedure.



Fig. 17. Limitation. Our network may have difficulty distinguishing between nearby surfaces, and incorrectly renders them as a continuous surface. This problem arises from the ambiguity between typical sampling space and surface holes.

There is an interesting tradeoff between speed and shading locality that we plan to explore more in the future. Local shading effects, i.e., ambient, diffuse and specular can be learned at the patch level, while global shading, like shadows or reflections, are significantly harder and require learning non-local interactions. One research avenue is to incorporate transformers for learning inter-patches dependencies. Another challenging direction is to improve rendering fine details including sharp features. These, however, are still challenging also for slower methods that reconstruct surfaces from sparse point clouds, let alone for instant rendering.

REFERENCES

- Panos Achlioptas, Olga Diamanti, Ioannis Mitliagkas, and Leonidas Guibas. 2018. Learning representations and generative models for 3d point clouds. In *International conference on machine learning*. PMLR, 40–49.
- Kara-Ali Aliev, Dmitry Ulyanov, and Victor Lempitsky. 2019. Neural point-based graphics. *arXiv preprint arXiv:1906.08240* 2, 3 (2019), 4.
- Matthew Berger, Andrea Tagliasacchi, Lee M Seversky, Pierre Alliez, Gael Guennebaud, Joshua A Levine, Andrei Sharf, and Claudio T Silva. 2017. A survey of surface reconstruction from point clouds. In *Computer Graphics Forum*, Vol. 36. Wiley Online Library, 301–329.
- Fausto Bernardini, Joshua Mittleman, Holly Rushmeier, Claudio Silva, and Gabriel Taubin. 1999. The ball-pivoting algorithm for surface reconstruction. *IEEE transactions on visualization and computer graphics* 5, 4 (1999), 349–359.

- Mario Botsch and Leif Kobbelt. 2003. High-quality point-based rendering on modern GPUs. In *11th Pacific Conference on Computer Graphics and Applications, 2003. Proceedings. IEEE*, 335–343.
- Ruojin Cai, Guandao Yang, Hadar Averbuch-Elor, Zekun Hao, Serge Belongie, Noah Snavely, and Bharath Hariharan. 2020. Learning Gradient Fields for Shape Generation. In *Proceedings of the European Conference on Computer Vision (ECCV)*.
- Wenzheng Chen, Jun Gao, Huan Ling, Edward Smith, Jaakko Lehtinen, Alec Jacobson, and Sanja Fidler. 2019. Learning to Predict 3D Objects with an Interpolation-based Differentiable Renderer. In *Advances In Neural Information Processing Systems*.
- Xuelin Chen, Daniel Cohen-Or, Baoquan Chen, and Niloy J. Mitra. 2021. Towards a Neural Graphics Pipeline for Controllable Image Generation. *Computer Graphics Forum* 40, 2 (2021).
- Blender Online Community. 2021. *Blender - a 3D modelling and rendering package*. Blender Foundation, Blender Institute, Amsterdam. <http://www.blender.org>
- Peng Dai, Yinda Zhang, Zhuwen Li, Shuaicheng Liu, and Bing Zeng. 2020. Neural point cloud rendering via multi-plane projection. In *Proceedings of the IEEE/CVF Conference on Computer Vision and Pattern Recognition*. 7830–7839.
- Herbert Edelsbrunner and Ernst P Mücke. 1994. Three-dimensional alpha shapes. *ACM Transactions on Graphics (TOG)* 13, 1 (1994), 43–72.
- Rinon Gal, Amit Bermanto, Hao Zhang, and Daniel Cohen-Or. 2020. MRGAN: Multi-Rooted 3D Shape Generation with Unsupervised Part Disentanglement. *arXiv preprint arXiv:2007.12944* (2020).
- Paul Guerrero, Yanir Kleiman, Maks Ovsjanikov, and Niloy J. Mitra. 2018. PCPNet: Learning Local Shape Properties from Raw Point Clouds. *Computer Graphics Forum* 37, 2 (2018), 75–85.
- Rana Hanocka, Gal Metzger, Raja Giryes, and Daniel Cohen-Or. 2020. Point2Mesh: A Self-Prior for Deformable Meshes. *ACM Trans. Graph.* 39, 4, Article 126 (July 2020), 12 pages. <https://doi.org/10.1145/3386569.3392415>
- Pedro Hermosilla, Sebastian Maisch, Tobias Ritschel, and Timo Ropinski. 2019. Deep-learning the Latent Space of Light Transport. In *Computer Graphics Forum*, Vol. 38. Wiley Online Library, 207–217.
- Amir Hertz, Rana Hanocka, Raja Giryes, and Daniel Cohen-Or. 2020. PointGMM: a Neural GMM Network for Point Clouds. In *Proceedings of the IEEE/CVF Conference on Computer Vision and Pattern Recognition*. 12054–12063.
- Hugues Hoppe, Tony DeRose, Tom Duchamp, John McDonald, and Werner Stuetzle. 1992. Surface reconstruction from unorganized points. In *Proceedings of the 19th annual conference on Computer graphics and interactive techniques*. 71–78.
- Hui Huang, Dan Li, Hao Zhang, Uri Ascher, and Daniel Cohen-Or. 2009. Consolidation of unorganized point clouds for surface reconstruction. *ACM transactions on graphics (TOG)* 28, 5 (2009), 1–7.
- Xun Huang and Serge Belongie. 2017. Arbitrary style transfer in real-time with adaptive instance normalization. In *Proceedings of the IEEE International Conference on Computer Vision*. 1501–1510.
- James T Kajiya. 1986. The rendering equation. In *Proceedings of the 13th annual conference on Computer graphics and interactive techniques*. 143–150.
- Tero Karras, Samuli Laine, and Timo Aila. 2019. A style-based generator architecture for generative adversarial networks. In *Proceedings of the IEEE/CVF Conference on Computer Vision and Pattern Recognition*. 4401–4410.
- Michael Kazhdan, Matthew Bolitho, and Hugues Hoppe. 2006. Poisson surface reconstruction. In *Proceedings of the fourth Eurographics symposium on Geometry processing*, Vol. 7.
- Michael Kazhdan and Hugues Hoppe. 2013. Screened poisson surface reconstruction. *ACM Transactions on Graphics (ToG)* 32, 3 (2013), 1–13.
- Maria Kolos, Artem Sevastopolsky, and Victor Lempitsky. 2020. TRANSPR: Transparency Ray-Accumulating Neural 3D Scene Point Renderer. *arXiv preprint arXiv:2009.02819* (2020).
- Chun-Liang Li, Manzil Zaheer, Yang Zhang, Barnabas Poczos, and Ruslan Salakhutdinov. 2018. Point cloud gan. *arXiv preprint arXiv:1810.05795* (2018).
- Gal Metzger, Rana Hanocka, Raja Giryes, and Daniel Cohen-Or. 2020. Self-Sampling for Neural Point Cloud Consolidation. *arXiv preprint arXiv:2008.06471* (2020).
- Gal Metzger, Rana Hanocka, Denis Zorin, Raja Giryes, Daniele Panozzo, and Daniel Cohen-Or. 2021. Orienting Point Clouds with Dipole Propagation. (2021).
- Niloy J Mitra and An Nguyen. 2003. Estimating surface normals in noisy point cloud data. In *Proceedings of the nineteenth annual symposium on Computational geometry*. 322–328.
- Patrick Mullen, Fernando De Goes, Mathieu Desbrun, David Cohen-Steiner, and Pierre Alliez. 2010. Signing the unsigned: Robust surface reconstruction from raw pointsets. In *Computer Graphics Forum*, Vol. 29. Wiley Online Library, 1733–1741.
- Oliver Nalbach, Elena Arabadzhiyska, Dushyant Mehta, H-P Seidel, and Tobias Ritschel. 2017. Deep shading: convolutional neural networks for screen space shading. In *Computer graphics forum*, Vol. 36. Wiley Online Library, 65–78.
- Thu Nguyen-Phuoc, Chuan Li, Stephen Balaban, and Yong-Liang Yang. 2018. Rendernet: A deep convolutional network for differentiable rendering from 3d shapes. *arXiv preprint arXiv:1806.06575* (2018).
- Marie-Julie Rakotosaona, Vittorio La Barbera, Paul Guerrero, Niloy J Mitra, and Maks Ovsjanikov. 2020. Pointcleannet: Learning to denoise and remove outliers from dense point clouds. In *Computer Graphics Forum*, Vol. 39. Wiley Online Library, 185–203.
- Olaf Ronneberger, Philipp Fischer, and Thomas Brox. 2015. U-net: Convolutional networks for biomedical image segmentation. In *International Conference on Medical image computing and computer-assisted intervention*. Springer, 234–241.
- Takafumi Saito and Tokiichiro Takahashi. 1990. Comprehensible rendering of 3-D shapes. In *Proceedings of the 17th annual conference on Computer graphics and interactive techniques*. 197–206.
- Nico Schertler, Bogdan Savchynskyy, and Stefan Gumhold. 2017. Towards globally optimal normal orientations for large point clouds. In *Computer Graphics Forum*, Vol. 36. Wiley Online Library, 197–208.
- Andrei Sharf, Thomas Lewiner, Ariel Shamir, Leif Kobbelt, and Daniel Cohen-Or. 2006. Competing fronts for coarse-to-fine surface reconstruction. In *Computer Graphics Forum*, Vol. 25. Wiley Online Library, 389–398.
- Matthew Tancik, Pratul P. Srinivasan, Ben Mildenhall, Sara Fridovich-Keil, Nithin Raghavan, Utkarsh Singhal, Ravi Ramamoorthi, Jonathan T. Barron, and Ren Ng. 2020. Fourier Features Let Networks Learn High Frequency Functions in Low Dimensional Domains. *NeurIPS* (2020).
- Chulin Xie, Chuxin Wang, Bo Zhang, Hao Yang, Dong Chen, and Fang Wen. 2021. Style-based Point Generator with Adversarial Rendering for Point Cloud Completion. *arXiv preprint arXiv:2103.02535* (2021).
- Guandao Yang, Xun Huang, Zekun Hao, Ming-Yu Liu, Serge Belongie, and Bharath Hariharan. 2019. Pointflow: 3d point cloud generation with continuous normalizing flows. In *Proceedings of the IEEE International Conference on Computer Vision*. 4541–4550.
- Wang Yifan, Felice Serena, Shihao Wu, Cengiz Öztireli, and Olga Sorkine-Hornung. 2019a. Differentiable surface splatting for point-based geometry processing. *ACM Transactions on Graphics (TOG)* 38, 6 (2019), 1–14.
- Wang Yifan, Shihao Wu, Hui Huang, Daniel Cohen-Or, and Olga Sorkine-Hornung. 2019b. Patch-based progressive 3d point set upsampling. In *Proceedings of the IEEE Conference on Computer Vision and Pattern Recognition*. 5958–5967.
- Lequan Yu, Xianzhi Li, Chi-Wing Fu, Daniel Cohen-Or, and Pheng-Ann Heng. 2018a. Ecnnet: an edge-aware point set consolidation network. In *Proceedings of the European Conference on Computer Vision (ECCV)*. 386–402.
- Lequan Yu, Xianzhi Li, Chi-Wing Fu, Daniel Cohen-Or, and Pheng-Ann Heng. 2018b. Pu-net: Point cloud upsampling network. In *Proceedings of the IEEE Conference on Computer Vision and Pattern Recognition*. 2790–2799.
- Wentao Yuan, Tejas Khot, David Held, Christoph Mertz, and Martial Hebert. 2018. Pcn: Point completion network. In *2018 International Conference on 3D Vision (3DV)*. IEEE, 728–737.
- Matthias Zwicker, Hanspeter Pfister, Jeroen Van Baar, and Markus Gross. 2001. Surface splatting. In *Proceedings of the 28th annual conference on Computer graphics and interactive techniques*. 371–378.